Article

Evaluation of Nb_2O_5 ceramic nanofibers efficacy to promote CO_2 photoconversion.

Prado, A. C.F. [1,2], Malafatti, J. O. D [1,3], Oliveira, J. A. [1,4], Ribeiro, C [1], Joya, M. R [5,*], Luz, A. P. [1], and Paris, E. C [1,*]

[1] Nanotechnology National Laboratory for Agriculture (LNNA), Embrapa Instrumentação, XV de Novembro St., 1452, 13560-970, São Carlos, SP, Brazil; caue.ribeiro@embrapa.br,Analuz@ufscar.br.elaine.paris@embrapa.br
[2] Department of Materials Engineering, Federal University of São Carlos, Rod. Washington Luís, Km 235, 13.565-905, São Carlos, SP, Brazil;anapradol@gmail.com
[3] Department of Chemistry, Federal University of São Carlos, Rod. Washington Luís, Km 235, 13.565-905, São Carlos, SP, Brazil; jmalafatti@hotmail.com
[4] Department of Chemical Engineering, Federal University of São Carlos, Rod. Washington Luís, Km 235, 13.565-905, São Carlos, SP, Brazil.; jessicarianeoliveira@hotmail.com
[5] Departamento de Física, Facultad de Ciencias, Universidad Nacional de Colombia-Bogota, Carrera 30 Calle 45-03, 111321, Bogota, Colombia; mrinconj@unal.edu.co
* Correspondence: mrinconj@unal.edu.co (M.R.J.); elaine.paris@embrapa.br(E.C.P)

Abstract: The increase in global warming due to NO_x, CO_2, and CH_4 harmfully different ecosystems and significantly prejudice world life. A promising methodology in this sense is the pollutant conversion into valuable chemicals from photocatalytic processes by reusable photocatalyst. In this way, the present work aimed to produce a Nb_2O_5 photocatalyst nanofibers system to convert CO_2 by the electrospinning method. Based on the collected data, the nanofibers calcination at 600°C for 2 h resulted in the best condition to obtain a homogeneous surface with an average diameter of 84 nm. As a result, the Nb_2O_5 nanofibers converted CO_2 mostly into CO and CH_4, reaching values around 8.5 mol g^{-1} and 0.55 mol g^{-1}, respectively.

Keywords: Nb_2O_5, CO_2 conversion; Photocatalysis; Electrospinning; Nanofibers.

1. Introduction

Diverse methodologies have been developed to remove pollutants from different media to address the growing concern with environmental quality. In this vein, heterogeneous photocatalysis has gained attention due to its capacity to remove and degrade contaminants, photocatalytic recovery, and reuse in new cycles [1,2] CO_2 photoreduction is especially emerging because of the need to decrease greenhouse gases and diminish their consequent harmful environmental impacts [3].Photocatalysis is based on complex catalytic reactions that enable the formation of specific products such as methanol, methane, carbon monoxide, formic acid, etc [4].In order to improve the photocatalytic stability, production rate, and selectivity, different catalysts systems have been studied, such as TiO_2[5],ZnO[6], and WO_3 [7].

Zeng *et al.* [8] investigated the incorporation of Cu_2O nanowires in titanium carbide (Ti_3C_2). These authors confirmed the enhancement of the material efficiency to convert Cu_2O into methanol, inducing an increase in the production around 8.25 times compared to the isolated Cu_2O nanowires. This performance improved the charge carrier's transport and reduced the bandgap (from 2.2 to 2.02 eV) that optimizes the light absorption capacity and modifies the charge recombination processes. Ye *et al.* [9] proposed the design of nano-tubes bismuth-based heterostructure photocatalysts for CO_2 photoconversion. Among the tested BiOX type heterostructures (with X equal to Cl, Br, or I), BiOI showed the best performance under visible irradiation, as its bandgap was

Preprints (www.preprints.org) | NOT PEER-REVIEWED | Posted: 22 October 2021 doi:10.20944/preprints202110.0333.v1

the smallest one (1.7 - 1.8 eV), favoring the CO_2 photoreduction in CO and CH_4 (19.82 mol g^{-1} h^{-1} and 0.22 mol g^{-1} h^{-1}, respectively). However, even though this narrow bandgap range facilitates the recombination of the photo-generated pairs, such a feature may also lead to photocatalytic activity loss.

Niobium pentoxide (Nb_2O_5) is a semiconductor that has received attention due to its similar features to TiO_2 and promising performance when applied in CO_2 photoconversion [10–12]. Silva *et al.* [12] studied the photocatalytic activity of Nb_2O_5 particles after modifying their surface with peroxo groups. The authors observed that selectivity and photocatalytic activity were related to the surface acidity of the nanoparticles. Thus, high surface acidity led to CO_2 conversion into CO, HCOOH, and CH_3COOH, whereas low acidity induced mainly CH_4 formation. Although niobium-based materials are promising alternatives to be applied in CO_2 photoconversion, it was not found in the literature the use of Nb_2O_5 ceramic nanofibers for this application. However, photocatalysis using nanofibers has been employed to degrade pollutants [13,14] due to their porous control and homogeneous diameter distribution that enhance the availability of catalytic sites aside from the improvement in the photocatalyst activity due to its preferentially directed form.

To the best of our knowledge, no investigations have been carried out considering the use of polyvinyl alcohol (PVA, which is highly soluble in water) as a polymeric precursor for the Nb_2O_5 fibers synthesis. Based on these aspects, the present work addressed the Nb_2O_5 ceramic nanofibers synthesis and characterization for CO_2 photoreduction, considering the electrospinning method and using polyvinyl alcohol as a precursor under different annealing conditions.

2. Materials and Methods

2.1. Synthesis of Nb_2O_5 fibers

For producing ceramic fibers, polyvinyl alcohol (PVA, Mw 50000, Sigma Aldrich, 99.9% purity) and niobium ammonia oxalate (OAN, Mw 353.02, donated by CBMM-Brazil) were used. First, PVA was solubilized in deionized water to obtain a 20% (w V^{-1}) concentration solution. In parallel, the OAN precursor salt was solubilized in deionized water to obtain a concentration of 40% (w w^{-1}). The solutions were then mixed and homogenized under magnetic stirring for about 30 minutes. Finally, the obtained fibers were subjected to thermal treatment, varying the temperature from 400°C to 900°C for 2 h, and heating rate of 1 or 10°C min^{-1}, based on adaptations from the literature [15]

2.2. Characterization

Thermogravimetric analysis (TGA) was performed on precursor fiber to verify the events of polymer matrix degradation and mass loss. The equipment used was the TA Instruments, model Q500. The fiber was heated in a temperature range between 30 and 900ºC, with a heating rate of 10ºC min^{-1} and a synthetic air atmosphere with a flow rate of 10 mL h^{-1}. The scanning electron microscopy (SEM) technique allowed the obtainment of images that provide Nb_2O_5 fibers information on the shape, diameter, and distribution, using a JEOL® model 6701F microscope. In addition, the average diameters of the sample were measured with the aid of Image J software.

2.3. Immobilization of Nb_2O_5 ceramic fibers

The selected photocatalytic materials were immobilized on glass slides (2 x 2 cm) which were previously cleaned in a sonicator bath with Extran, water, acetone, ethanol, and water, subsequently. From then, the fibers were added to a beaker containing 5 mL of ethanol for dispersion in a thermostatic bath at room temperature (25°C) for 30 minutes. After this procedure, the glass slide was placed over a heating plate kept at

Preprints (www.preprints.org) | NOT PEER-REVIEWED | Posted: 22 October 2021 doi:10.20944/preprints202110.0333.v1

50°C. Finally, the suspension was slowly dropped over the substrate surface until the formation of a film along the entire length of the glass slide.

2.4. Evaluation of CO_2 gaseous photoconversion

The immobilized photocatalysts were inserted into the cavity of a stainless steel reactor. The system was purged with ultra-pure gas containing CO_2 and water vapor for 20 min before the experiment. Afterward, the reactor was sealed and exposed to UV-C irradiation (TUV Philips 18 W mercury lamp, 254 nm) for 6 h at room temperature. Aliquots (300 μL) were removed every hour and analyzed in a gas chromatograph (GC), CG Varian model CP - 3800 equipped with a thermal conductivity detector (TCD) and a flame ionization detector (FID), using a column (HayeSep N (0.5m x 1.8")) with a flow rate of 30 mL min^{-1} for H_2, 300 mL min^{-1} for air, and 30 mL min^{-1} for N_2, using argon as carrier gas. The injector temperature was set at 150ºC, while the TCD and FID detector temperatures were 200ºC and 150ºC, respectively.

3. Results

3.1. Optimization of the Nb_2O_5 ceramic fibers

The thermogravimetric analysis indicated the mass loss and the organic degradation events when the fibers were subjected to thermal heating. Figure 1 shows the PVA fiber degradation behavior in the range from 70ºC to 800ºC. As observed, the prepared polymeric fibers showed mass losses up to 480ºC. The main thermal events were identified at 150ºC and 250ºC due to the adsorbed water removal from the sample surface (#1) and the beginning of polymer degradation with the elimination of water molecules (#2). Furthermore, at 270°C, the PVA main chain degradation began (#3), with pyrolysis and PVA degradation events also being verified between 320ºC and 500ºC (#4). Results similar to those shown in Figure 1 are reported in the literature [16,17], showing the PVA polymer matrix degradation.

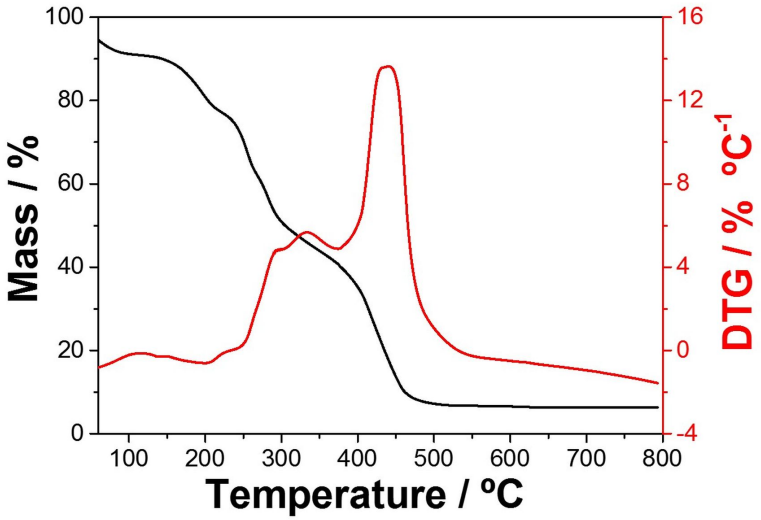

Figure 1. Thermogravimetric profile of the evaluated PVA:OAN fibers.

Once verified the PVA degradation behavior against heat treatment, the morphology of the Nb_2O_5 fibers was analyzed. Thus, fibers were submitted in an annealing treatment from 400ºC to 900ºC for 2 h with a fixed heating rate of 10 ºC min^{-1}. The SEM images results (Figure 2) show the fiber format leakage and the consequent formation of the particles with calcination temperature increasing. The predominance of fiber morphology is observed at temperatures from 400ºC to 700ºC, and agglomerates at higher temperatures. Additionally, the fibers average diameter obtained from 400°C to 700°C

Preprints (www.preprints.org) | NOT PEER-REVIEWED | Posted: 22 October 2021 doi:10.20944/preprints202110.0333.v1

was 170 nm, 140 nm, 150 nm, and 120 nm, respectively. However, when the temperature was raised to 800ºC, the formation of a more significant number of shapeless particles with an average diameter of 135 nm was verified. Furthermore, the fiber loss format was observed after 900ºC that led to the particulate material formation.

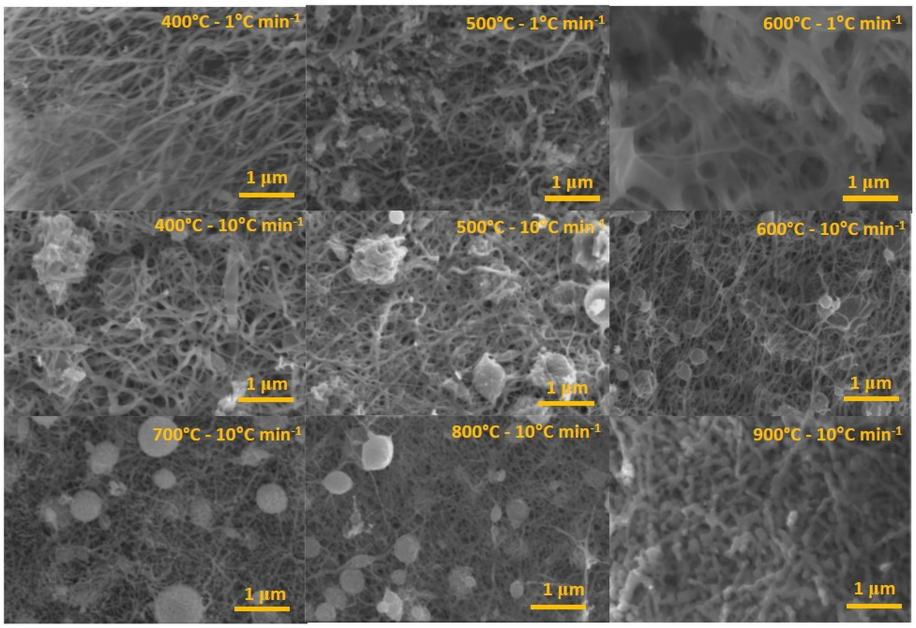

Figure 2. SEM images of the Nb_2O_5 fibers after the thermal treatments at different temperatures (400 – 900°C), using a heating rate of 1°C min^{-1} and 10°C min^{-1}.

The mentioned morphological characteristics are due to the increasing temperature. Consequently, the energy supplied favors the Nb_2O_5 fibers coalescence effect, resulting in a fiber losing initial shape and introducing new particles, inducing growth until thermodynamic equilibrium [18,19]. Furthermore, according to Figure 2, samples treated at 400°C, 500°C, and 600°C using a heating rate of 1°C min^{-1} showed fiber-like morphology with mean diameters of 280 nm, 130 nm, and 84 nm, respectively. Thus, fibers obtained at 600°C showed greater homogeneity and smaller diameter when compared to those obtained at 10°C min^{-1}. The obtained results are similar to the literature [20,21], which also verified morphological differences related to the heating rate during the annealing process; this step is essential for morphology formulation. Besides that, to the lowest heating rate, a more regular aspect was defined for fibers without pores, attributed to greater control of polymeric matrix degradation.

In order to verify the heating rate effects, the range of 400 – 600°C was chosen to observe the structural changes due to PVA matrix degradation and Nb_2O_5 calcination. Figure 3 shows the XRD diffractograms performed for Nb_2O_5 ceramic fibers. At this temperature, the low heating rate of 1°C min^{-1} (Figure 3a) contributed to the structural Nb_2O_5 phase formation that showed only the orthorhombic phase characteristic peaks (JCPDS 28-317), corroborating to the literature results [22]. On the other hand, regarding the temperatures of 400°C and 500°C, the absence of the Nb_2O_5 peaks was observed, being detected amorphous halos, similar to pure PVA. Thus, the temperature of 600°C was the minimum for the desirable Nb_2O_5 phase formation.

Preprints (www.preprints.org) | NOT PEER-REVIEWED | Posted: 22 October 2021 doi:10.20944/preprints202110.0333.v1

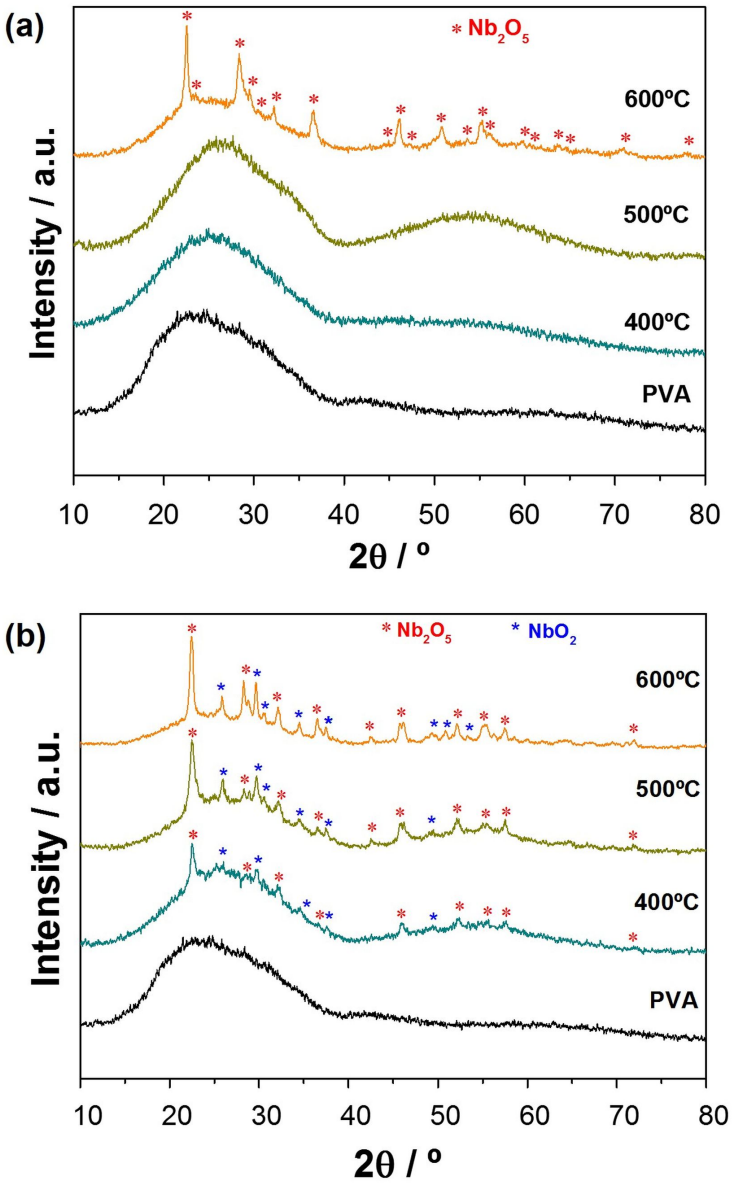

Figure 3. X-ray profiles of Nb_2O_5 fibers after thermal treatments at 400°C, 500°C, and 600°C under a heating rate of (a) 1°C min^{-1} and (b)10°Cmin^{-1}.

In order to verify the effects of the heating rate in the structural characteristics, the range of 400 – 600°C was chosen to observe the PVA matrix degradation impacts during the Nb_2O_5 calcination step. The diffractograms in Figure 3b prove the oxide formation at 400, 500, and 600°C, identifying the orthorhombic preferential Nb_2O_5 phase (JCPDS card n° 28-317). In addition, the presence of a secondary NbO_2 phase (JCPDS n° 19-0859) was also identified, with more intense peaks located at 26.73°, 30.00° and 49.62° (Figure 3b), presented in all temperatures intervals from 400 – 600°C. Thus, comparing the diffractograms obtained for the same temperatures in a heating rate of 10°C min^{-1} with 1°C min^{-1} (Figure 3b), it is noted that the lower rate decreased the polymeric degradation rate and favored a more controlled thermal treatment since occurred the organic matrix elimination and the structural arrangement formation of the ceramic fibers. Furthermore, the heating rate increased the PVA fiber faster degradation, changing the atmosphere with high CO_2 elimination and reducing the atmosphere's oxidizing capacity. Yun et al. [23] obtained different niobium oxide phases, TT-Nb_2O_5 (pseudohexagonal phase), TT-Nb_2O_5/M-NbO_2, and M-NbO_2 (monoclinic phase) from

Preprints (www.preprints.org) | NOT PEER-REVIEWED | Posted: 22 October 2021 doi:10.20944/preprints202110.0333.v1

samples calcined at temperatures of 700, 800, and 1000°C under N_2 reducing atmosphere. The authors identified that the transformations from Nb_2O_5 to NbO_2 phase occurred during the temperature increase and a decrease in the Nb valence state from 5+ to 4+, a characteristic presented by transition metal oxides, such as the Ta_2O_5 and V_2O_5.

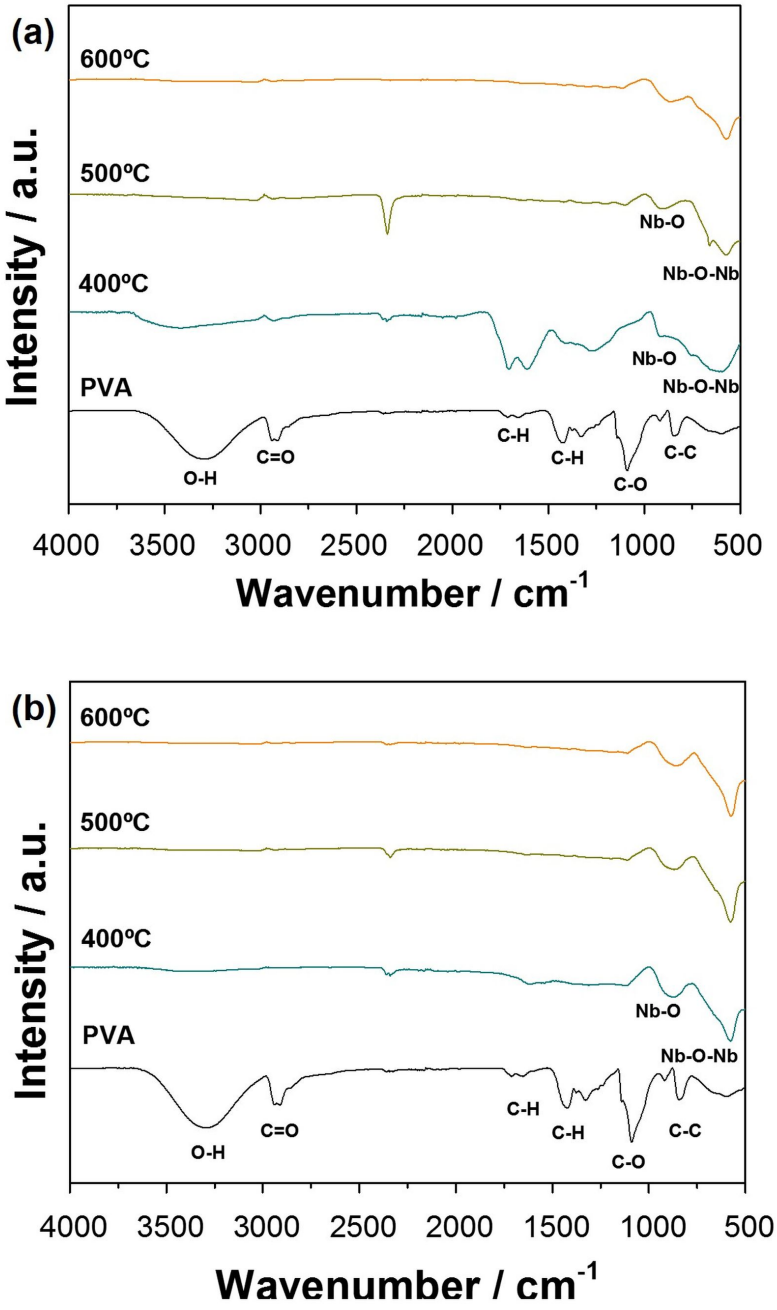

Figure 4. FTIR profiles of PVA and Nb_2O_5 ceramic fibers after thermal treatments at 400°C, 500°C or 600°C at a heating rate of (a) 1°C min^{-1} and (b) 10°C min^{-1}.

In order to further understand the structural properties of the ceramic nanofibers, FTIR analysis was performed for different heating rates to identify the presence of residual organic material in the samples after annealing. Figure 4a shows the results of the FTIR analysis for the fibers calcined at a heating rate of 1°C min^{-1}. Only the highest temperature of 600°C indicated the presence of pure Nb_2O_5 bands located at 872 cm^{-1} referring to bonds (Nb=O) and in 613 cm^{-1} associated with the bonds (Nb-O-Nb) [24,25]. The PVA polymeric matrix presents vibration bonds located in positions at 3314 cm^{-1}

Preprints (www.preprints.org) | NOT PEER-REVIEWED | Posted: 22 October 2021 doi:10.20944/preprints202110.0333.v1

and 3332 cm^{-1} (O-H), 2917 cm^{-1} (C=O), 1500 cm^{-1} (C-H), 1000 cm^{-1} (C-O), and around 800 cm^{-1} (C-C) [26]. The same result is observed at temperatures of 400°C and 500°C.

For the fibers spectra obtained at the rate of 10°C min-1 (Figure 4b) is verified that even at the lowest temperatures of 400°C and 500°C, there is only the appearance of typical Nb-O bands. These results corroborate the data obtained from the XRD diffractograms (Figure 3), indicating that a minor decrease in the polymeric part elimination occurred when a lower heating rate was used, preventing the crystalline ceramic fiber formation at lower temperatures.

The fibers calcined at 1°C min^{-1} are different from those treated at 10°C min^{-1}, especially for the 400°C, showing that the vibration modes of organic molecules are much more evident. However, with the heating rate of 10°C min^{-1}, the fibers still have organic residues attributed to the rapid decomposition. Thus, these arrangements were not so well organized, influencing the inexistence of some vibrational modes. In this way, decreasing the heating rate allows the samples to be exposed to the temperature for more extended periods, leading to the highest structural organization. In order to evaluate the optical properties of the samples, diffuse reflectance spectroscopy (DRS) analysis was performed. Both fibers calcined at 600°C presented a similar bandgap between 3.6 (10°Cmin^{-1}) and 3.8 eV(1°Cmin^{-1}), which values are close to the expected range reported in the literature for Nb_2O_5 [27].

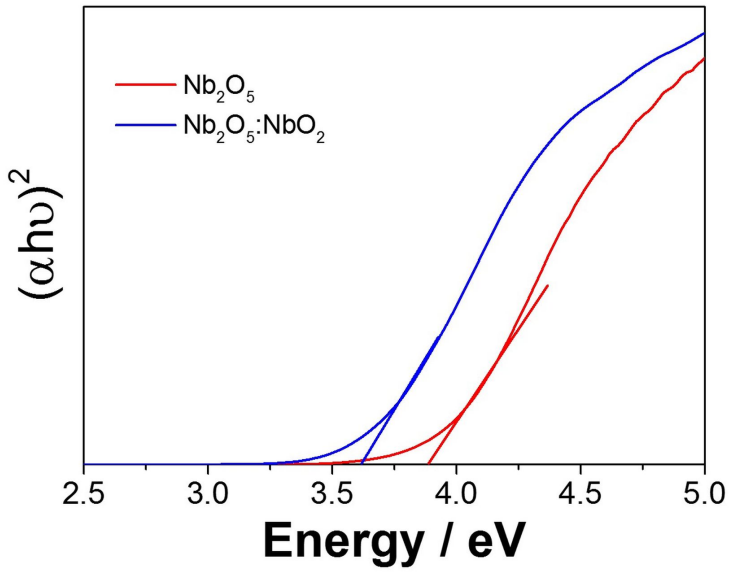

Figure 5. Diffuse reflectance spectroscopy (DRS) of fibers annealed at 600°C for 2 h, with heating rates of 1 and 10°C min^{-1}.

After the Nb_2O_5 samples structural and morphological characterization, the fibers obtained at 600°C, 1°C min^{-1}, and 10°C min^{-1} were selected for the CO_2 photoreduction. These systems presented the elimination of the organic precursor and the niobium oxide phases.

3.2. Photocatalytic conversion of CO_2

Nb_2O_5 and Nb_2O_5:NbO_2 fibers were selected to verify the effects of photocatalytic activity on the gaseous CO_2 photoconversion. The kinetics shown in Figure 6a indicates the concentration of CO (μmol g^{-1}) produced during 6 h for each photocatalyst system. The Nb_2O_5 fiber produced more CO in all intervals, increasing from 2.0 mol g^{-1} (1 h) to 8.2 μmol g^{-1} after 6 h. On the other hand, the Nb_2O_5:NbO_2 photocatalyst produced less CO, reaching 3.8 mol g^{-1} in 6 h of reaction. This value was 46% lower when compared to pure Nb_2O_5 in the same period to produce CO. With this result is concluded that pure Nb_2O_5 realized a better photocatalyst system performance for the CO production. In

Preprints (www.preprints.org) | NOT PEER-REVIEWED | Posted: 22 October 2021 doi:10.20944/preprints202110.0333.v1

this way, the NbO_2 second phase prejudices the photocatalytic performance of the pure Nb_2O_5 catalyst.

Catalytic properties are strongly influenced by the presence of acidic and basic sites on the catalyst surface. Considering this question and according to Lewis theory, Nb^{5+} ions have electron acceptor potential, acting as an acid, while O^{2-} anions act like a basic receiver. Therefore, the acid-base interactions that occur on the surface of Nb_2O_5 and the CO_2 reaction can influence the formation of activated complexes. Regarding the second phase, NbO_2, which presents a narrow bandgap of about 0.7 eV, presents an electronic configuration different from Nb_2O_5, being $4d^1$ and $4d^0$, respectively. The electron present in the 4d electronic layer can be donated or shared, facilitating the oxygen reduction reactions and consequently decreasing the oxidation number of the NbO_2 compound, which can influence the decrease in the photocatalytic activity [28]. Thus, despite obtaining a material with a lower bandgap value, Nb_2O_5:NbO_2 (3.3 eV) compared to Nb_2O_5 (3.8 eV), as seen in Figure 5, the secondary phase can promote a higher recombination rate of the photogenerated pairs, strongly influencing the photocatalytic properties.

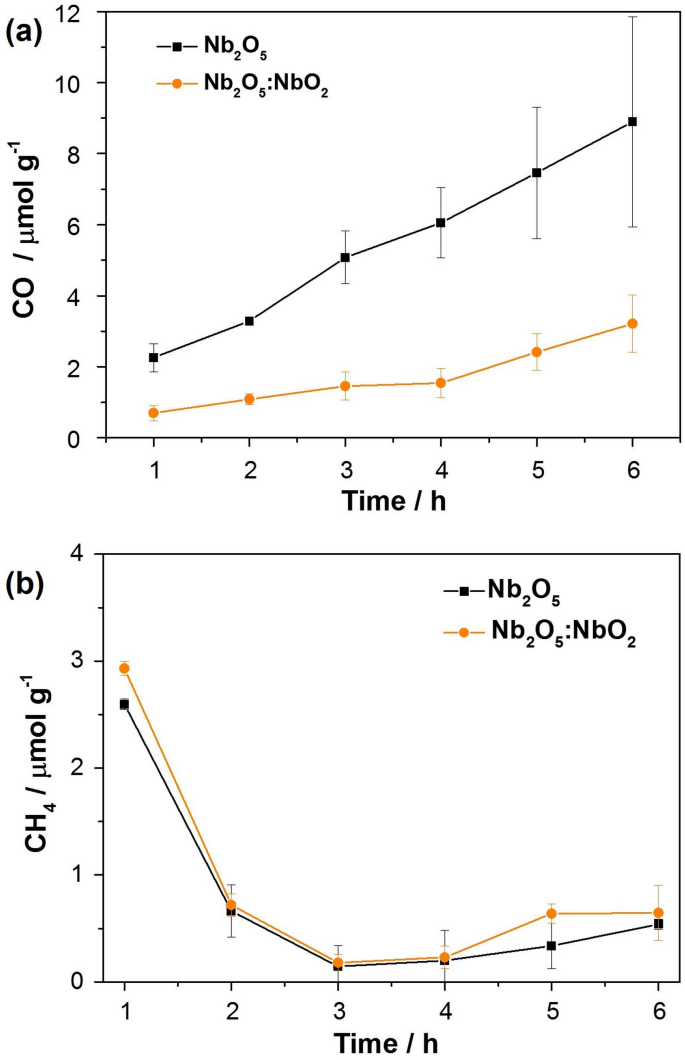

Figure 6. CO_2 gaseous photoreduction in (a) CO and (b) CH_4 during 6 h under UV-C irradiation.

Figure 6b shows the CH_4 production by Nb_2O_5 and Nb_2O_5:NbO_2 photocatalysts over 6 h, verified in the first hour of analysis an amount of 2.6 and 2.9 μmol g^{-1} of CH_4. However, the CH_4 concentration dropped abruptly in the second hour, remaining

Preprints (www.preprints.org) | NOT PEER-REVIEWED | Posted: 22 October 2021 doi:10.20944/preprints202110.0333.v1

practically constant (around 0.6 and 0.7 mol g^{-1}) for both materials. In this sense, it was observed that the different materials prepared based on niobium tend to produce CO preferentially. This behavior is justified because the CO_2 reduction mechanism requires two electrons to produce CO molecules and eight electrons for CH_4 formation. For this reason, the generation of CH_4 is much more complex [29]]. Furthermore, CO can strongly adsorb on the photocatalyst surface, and desorption of the process can significantly affect the yield of the CH_4 formation [30].

Studies reveal that the surface acidity of the photocatalyst can influence the selectivity of the products generated from CO_2 photoreduction [11,12]. The size of nanoparticles, composition of the photocatalysts can also influence the selectivity during the photoreduction reaction [31]. Nogueira et al. [4] proposed an interaction mechanism between the surface of Nb_2O_5 with CO_2 and the selectivity of products. When reaction medium pH is next to 5.5, part of the CO_2 molecules are HCO^{2-} ions, and CO_2 oxygen atoms with pairs of electrons can be transferred like Lewis bases. The Nb_2O_5 structure is composed of NbO_4 tetrahedral, forming NbO_4-H_2O structures in the presence of water vapor, which start to act as Lewis acid sites, receiving the oxygen electron pair from CO_2, enabling coordination with the photocatalyst surface. Similarly, the preferential CO production for the samples is due to the high oxygen interaction between the CO_2 molecules and photocatalyst active sites.

Preprints (www.preprints.org) | NOT PEER-REVIEWED | Posted: 22 October 2021 doi:10.20944/preprints202110.0333.v1

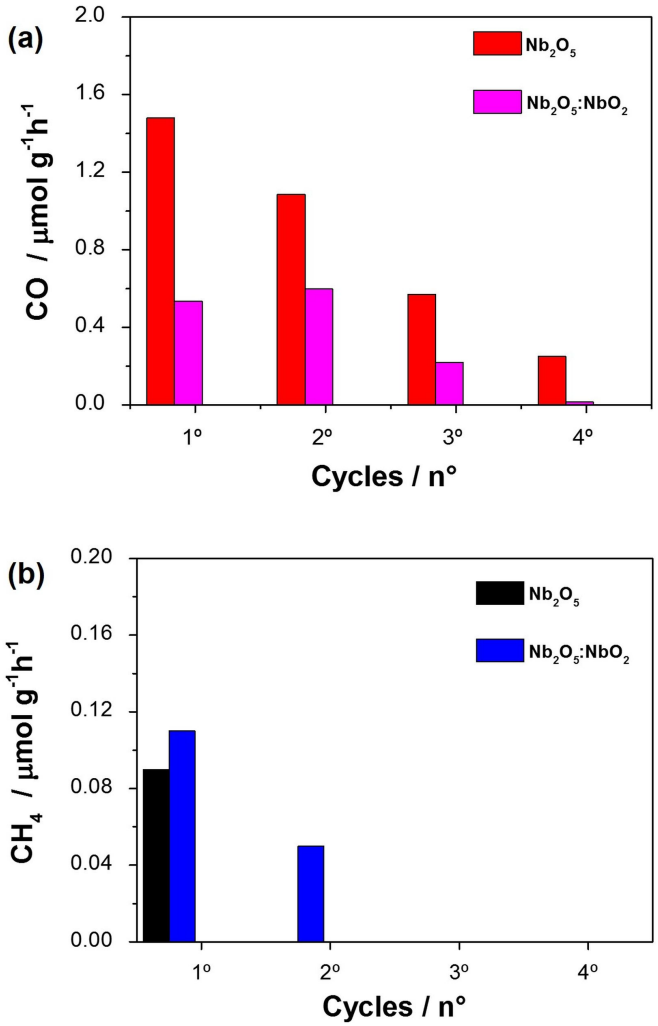

Figure 7. CO_2 conversion rate into (a) CO and (b) CH_4 products after a period of 6 h under UV-C irradiation, during 4 consecutive cycles.

After the first photocatalysis cycle of Nb_2O_5 and Nb_2O_5:NbO fibers, 3 reuse tests were performed to evaluate the stability of the samples. Figure 7 shows the production rate (mol g^{-1} h^{-1}) of CO and CH_4 per cycle, and a decrease in the formation of both products over the consecutive cycles is observed.

In Figure 7a, it is observed that Nb_2O_5 was the material that produced the highest CO concentration in all analysis cycles, being the only one that produced significant amounts up to the 4^{th} cycle. However, the Nb_2O_5:NbO_2 system, despite the lower yield, remained stable in the production of CO, preserving the photocatalytic activity until the 3^{rd} cycle in a relevant way. Thus, the secondary NbO_2 phase indicated a lower degree of deactivation of the catalytic sites than pure Nb_2O_5. The deactivation of catalytic sites is one of the fundamental parameters for CO_2 reduction [32]. The 4+ Nb oxidation state of NbO_2 under O_2 deficiency allows the formation of substitution defects in the Nb_2O_5 structure, allowing the NOX reduction from Nb^{5+} to Nb^{4+}, which can influence the production of electrons in the catalytic sites and favor the formation of products such as CH_4 before the catalytic site is deactivated from the niobium oxidation to the 5+ state [33].

In Figure 7b, it was verified that the Nb_2O_5:NbO2 system produced CH_4 in a 2nd reuse, maintaining about 50% of the amount observed in the previous cycle. This

behavior was due to preserving the photocatalytic activity of the intermediate CO, seen in Figure 7a. Thus, although the secondary NbO_2 phase in the Nb_2O_5 system decreases its overall photocatalytic performance, the presence of NbO_2 resulted in an enhanced capacity in the production of CH_4. Therefore, the production rate, selectivity of the products, and the maintenance of the photocatalytic performance in the reuse cycles are directly related to the niobium oxide phases.

4. Conclusions

The optimization of the calcination parameters showed Nb_2O_5 fibers with structural and morphology control. The use of different heating rates, 1and 10°C min^{-1}, induced the formation of two photocatalysts, Nb_2O_5 and Nb_2O_5:NbO_2, respectively. It was also verified that the annealing temperature has an important influence on the phase formation and morphology of fibers or particles. The CO_2 photoreduction was more efficient over Nb_2O_5 than Nb_2O_5:NbO_2, but CO and CH_4 were formed. Despite the lower photoreduction yield, a secondary NbO_2 phase allowed a photocatalytic performance better preservation. Therefore, ceramic nanofibers based on niobium oxide were effectively obtained, presenting photocatalytic activity in the CO_2 conversion into commercial interest products.

Author Contributions: "Conceptualization E.C.P.; Methodology, A.C.F.P, J.O.D.M and J.A.O.; Validation, A.C.F.P. and J.O.D.M Formal Analysis, A.C.F.P, J.O.D.M and J.A.O.; Investigation, A.C.F.P, J.O.D.M and J.A.O.; Resources, E.C.P. and C.R.; Data Curation, A.C.F.P.; Writing – Original Draft Preparation, A.C.F.P and J.O.D.M.; Writing – Review Editing, E.C.P, M.R.J, A.P.L.; Visualization, M.R.J.; Supervision, E.C.P.; Project Administration, E.C.P.; Funding Acquisition, M.R.J."

Acknowledgments: This study was financed in part by the Coordenação de Aperfeiçoamento de Pessoal de Nível Superior - Brasil (CAPES) - Finance Code 001 and grant number 88887.353014/2019-00. The authors acknowledge Embrapa (Grant Number 11.14.03.001.01.00), FINEP, SisNano, and AgroNano Network for financial support.

Conflicts of Interest: The authors declare no conflict of interest

References

1. Malafatti, J.O.D.; Moreira, A.J.; Sciena, C.R.; Silva, T.E.M.; Freschic, G.P.G.; Pereira, E.C.; Paris, E.C. Prozac® removal promoted by HAP:Nb_2O_5 nanoparticles system: By products, mechanism, and cytotoxicity assessment. *J. Environ. Chem. Eng.* 2020, 9, doi:10.1016/j.jece.2020.104820.
2. Paris, E.C.; Malafatti, J.O.D.; Sciena, C.R.; Junior, L.F.N.; Zenatti, A.; Escote, M.T.; Moreira, A.J.; Freschi, G.P.G. Nb_2O_5 nanoparticles decorated with magnetic ferrites for wastewater photocatalytic remediation.*Environ. Sci. Pollut. Res.* 2020, doi:10.1007/s11356-020-11262-5.
3. Izadpanah Ostad, M.; Niknam Shahrak, M.; Galli, F. Photocatalytic carbon dioxide reduction to methanol catalyzed by ZnO, Pt, Au, and Cu nanoparticles decorated zeolitic imidazolate framework-8. J. CO2 Util. 2021, 43, 101373, doi:10.1016/j.jcou.2020.101373.
4. Budzianowski, W.M.; Postawa, K. Renewable energy from biogas with reduced carbon dioxide footprint: Implications of applying different plant configurations and operating pressures. Renew. Sustain. Energy Rev. 2017, 68, 852–868, doi:10.1016/j.rser.2016.05.076.
5. Kočí, K.; Obalová, L.; Lacný, Z. Photocatalytic reduction of CO2 over TiO2 based catalysts. *Chem. Pap.* 2008, 62, 1–9, doi:10.2478/s11696-007-0072-x.
6. Oliveira, J.A.; Nogueira, A.E.; Gonçalves, M.C.P.; Paris, E.C.; Ribeiro, C.; Poirier, G.Y.; Giraldi, T.R. Photoactivity of N-doped ZnO nanoparticles in oxidative and reductive reactions. *Appl. Surf. Sci.* 2018, 433, 879–886, doi:10.1016/j.apsusc.2017.10.110.
7. Wang, H.; Zhang, L.; Wang, K.; Sun, X.; Wang, W. Enhanced photocatalytic CO2 reduction to methane over WO3·0.33H2O via Mo doping.*Appl. Catal. B Environ.* 2019, 243, 771–779, doi:10.1016/j.apcatb.2018.11.021.
8. Zeng, Z.; Yan, Y.; Chen, J.; Zan, P.; Tian, Q.; Chen, P. Boosting the Photocatalytic Ability of Cu2O Nanowires for CO2 Conversion by MXene Quantum Dots. *Adv. Funct. Mater.* 2019, 29, 1–9, doi:10.1002/adfm.201806500.
9. Ye, L.; Deng, Y.; Wang, L.; Xie, H.; Su, F. Bismuth-Based Photocatalysts for Solar Photocatalytic Carbon Dioxide Conversion. *ChemSusChem* 2019, 12, 3671–3701, doi:10.1002/cssc.201901196.
10. Lopes, O.F.; Paris, E.C.; Ribeiro, C. Synthesis of Nb2O5 nanoparticles through the oxidant peroxide method applied to organic pollutant photodegradation: A mechanistic study. Appl. Catal. B Environ. 2014, 144, 800–808, doi:10.1016/j.apcatb.2013.08.031.
11. Nogueira, A.E.; Silva, G.T.S.T.; Oliveira, J.A.; Lopes, O.F.; Torres, J.A.; Carmo, M.; Ribeiro, C. CuO Decoration Controls Nb 2 O 5 Photocatalyst Selectivity in CO 2 Reduction. ACS Appl. Energy Mater. 2020, acsaem.0c01047, doi:10.1021/acsaem.0c01047.

12. da Silva, G.T.S.T.; Nogueira, A.E.; Oliveira, J.A.; Torres, J.A.; Lopes, O.F.; Ribeiro, C. Acidic surface niobium pentoxide is catalytic active for CO2 photoreduction. Appl. Catal. B Environ. 2019, 242, 349–357, doi:10.1016/j.apcatb.2018.10.017.
13. Li, F.; Ruan, S.; Yin, Y.; Zhang, N.; Zhang, H.; Li, C.; Chen, Y. Facile synthesis of MnWO4/WO3 electrospun nanofibers as high performance visible-light driven photocatalysts. Mater. Lett. 2018, 229, 98–102, doi:10.1016/j.matlet.2018.06.118.
14. Szilágyi, I.M.; Santala, E.; Heikkilä, M.; Pore, V.; Kemell, M.; Nikitin, T.; Teucher, G.; Firkala, T.; Khriachtchev, L.; Räsänen, M.; et al. Photocatalytic properties of WO3/TiO2 core/shell nanofibers prepared by electrospinning and atomic layer deposition. Chem. Vap. Depos. 2013, 19, 149–155, doi:10.1002/cvde.201207037..
15. Nakane, K.; Morinaga, M.; Ogata, N. Formation of niobium oxide and carbide nanofibers from poly(vinyl alcohol)/niobium oxide composite nanofibers. J. Mater. Sci. 2013, 48, 7774–7779, doi:10.1007/s10853-013-7614-0.
16. Reguieg, F.; Ricci, L.; Bouyacoub, N.; Belbachir, M.; Bertoldo, M. Thermal characterization by DSC and TGA analyses of PVA hydrogels with organic and sodium MMT. Polym. Bull. 2020, 77, 929–948, doi:10.1007/s00289-019-02782-3.
17. Niazi, M.B.K.; Jahan, Z.; Ahmed, A.; Uzair, B.; Mukhtar, A.; Gregersen, Ø.W. Mechanical and thermal properties of carboxymethyl fibers (CMF)/PVA based nanocomposite membranes. J. Ind. Eng. Chem. 2020, 90, 122–131, doi:10.1016/j.jiec.2020.07.004.
18. Ferreira, E. de P.; Bessa, L.P.; Cardoso, V.L.; Reis, M.H.M. Influence of sintering temperature on the morphology of ceramic hollow fibers prepared from niobium pentoxide. Int. J. Appl. Ceram. Technol. 2019, 16, 781–790, doi:10.1111/ijac.13118.
19. Nakhowong, R. Fabrication and characterization of MnTiO3 nanofibers by sol-gel assisted electrospinning. Mater. Lett. 2015, 161, 468–470, doi:10.1016/j.matlet.2015.09.009.
20. Wan, M.; Zhu, H.; Zhang, S.G.; Jin, H.N.; Wen, Y.K.; Wang, L.N.; Zhang, M.; Du, M.L. Building block nanoparticles engineering induces multi-element perovskite hollow nanofibers structure evolution to trigger enhanced oxygen evolution. Electrochim. Acta 2018, 279, 301–310, doi:10.1016/j.electacta.2018.05.077.
21. Mohamadbeigi, N.; Angizi, S.; Sadrnezhaad, S.K.; Nikzad, M.J. Improving the multi-step fabrication approach of copper nanofiber networks based transparent electrode for achieving superb conductivity and transparency. Mater. Res. Express 2019, 6, doi:10.1088/2053-1591/ab128f.
22. Eblagon, K.M.; Malaika, A.; Ptaszynska, K.; Pereira, M.F.R.; Figueiredo, J.L. Impact of thermal treatment of nb2 o5 on its performance in glucose dehydration to 5-hydroxymethylfurfural in water. Nanomaterials 2020, 10, 1–24, doi:10.3390/nano10091685.
23. Yun, S.; Si, Y.; Shi, J.; Zhang, T.; Hou, Y.; Liu, H.; Meng, S.; Hagfeldt, A. Electronic Structures and Catalytic Activities of Niobium Oxides as Electrocatalysts in Liquid-Junction Photovoltaic Devices. Sol. RRL 2020, 4, 1–11, doi:10.1002/solr.201900430.
24. Aziz, S.B.; Brza, M.A.; Hamsan, M.H.; Kadir, M.F.Z.; Muzakir, S.K.; Abdulwahid, R.T. Effect of ohmic-drop on electrochemical performance of EDLC fabricated from PVA:dextran:NH4I based polymer blend electrolytes. J. Mater. Res. Technol. 2020, 9, 3734–3745, doi:10.1016/j.jmrt.2020.01.110.
25. Hass Caetano Lacerda, E.; Monteiro, F.C.; Kloss, J.R.; Fujiwara, S.T. Bentonite clay modified with Nb2O5: An efficient and reused photocatalyst for the degradation of reactive textile dye. J. Photochem. Photobiol. A Chem. 2020, 388, doi:10.1016/j.jphotochem.2019.112084.
26. Rad, L.R.; Momeni, A.; Ghazani, B.F.; Irani, M.; Mahmoudi, M.; Noghreh, B. Removal of Ni2+ and Cd2+ ions from aqueous solutions using electrospun PVA/zeolite nanofibrous adsorbent. Chem. Eng. J. 2014, 256, 119–127, doi:10.1016/j.cej.2014.06.066.
27. Park, H.; Lee, D.; Song, T. High capacity monoclinic Nb2O5 and semiconducting NbO2 composite as high-power anode material for Li-Ion batteries. J. Power Sources 2019, 414, 377–382, doi:10.1016/j.jpowsour.2019.01.015.
28. Peng, Y.; Lin, C.; Tang, M.; Yang, L.; Yang, Y.; Liu, J.; Huang, Z.; Li, Z. Niobium pentoxide ultra-thin nanosheets: A photocatalytic degradation and recyclable surface-enhanced Raman scattering substrate. Appl. Surf. Sci. 2020, 509, 145376, doi:10.1016/j.apsusc.2020.145376.
29. Inoue, T.; Fujishima, A.; Konishi, S.; Honda, K. Photoelectrocatalytic reduction of carbon dioxide in aqueous suspensions of semiconductor powders [3]. Nature 1979, 277, 637–638.
30. Raza, A.; Shen, H.; Haidry, A.A.; Sun, L.; Liu, R.; Cui, S. Studies of Z-scheme WO3-TiO2/Cu2ZnSnS4 ternary nanocomposite with enhanced CO2 photoreduction under visible light irradiation. J. CO2 Util. 2020, 37, 260–271,
31. Jia, J.; Wang, H.; Lu, Z.; O'Brien, P.G.; Ghoussoub, M.; Duchesne, P.; Zheng, Z.; Li, P.; Qiao, Q.; Wang, L.; et al. Photothermal Catalyst Engineering: Hydrogenation of Gaseous CO2 with High Activity and Tailored Selectivity. Adv. Sci. 2017, 4, doi:10.1002/advs.201700252.
32. Wang, S.; Han, X.; Zhang, Y.; Tian, N.; Ma, T.; Huang, H. Inside-and-Out Semiconductor Engineering for CO 2 Photoreduction: From Recent Advances to New Trends . Small Struct. 2021, 2, 2000061, doi:10.1002/sstr.202000061.
33. Mokrushin, A.S.; Simonenko, T.L.; Simonenko, N.P.; Gorobtsov, P.Y.; Kadyrov, N.C.; Simonenko, E.P.; Sevastyanov, V.G.; Kuznetsov, N.T. Chemoresistive Gas-Sensing Properties of Highly Dispersed Nb2O5 Obtained by Programmable Precipitation. J. Alloys Compd. 2021, 868, 159090, doi:10.1016/j.jallcom.2021.159090.